NLR-TP-2003-530

Static aeroelastic simulation using CFD, comparison with linear method
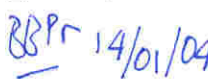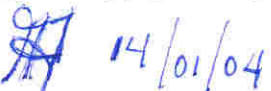
B.B. Prananta, J.J. Meijer and J. van Muijden

Approved by author:	Approved by project manager:	Approved by project managing department:
BBPr 14/01/04	14/01/04	16/01

Summary

This paper presents static aeroelastic simulations of fighter-type aircraft in transonic flow at various load factors. The linear approach of NASTRAN and NLR in-house developed ENFLOW computational aeroelastic simulation (CAS) system are employed in the simulation. ENFLOW CAS system, based on a CFD method employing the Euler/Navier-Stokes equations, solves the aeroelastic governing equations in a loosely-coupled manner. Prior to discussing the applications, several important aspects of the method will be described. Applications of the method are presented for fighter aircraft in a simple air-to-air configuration subjected to transonic flow. Two types of trimming have been used, the $[C_L] - [\alpha]$ trim strategy and $[C_L, C_{MP}] - [\alpha, \delta_\mathsf{H}]$ trim strategy. The efficiency and robustness of the method are shown by the quick convergence during the iteration to solve the sets of equations, i.e. aerodynamic, structural, and trim equations. As expected, for transonic flows, differences are observed between the results of ENFLOW and NASTRAN. Several possible causes of the differences are discussed. The deflection relative to the deflection at level flight compares well with the results of flight test.

Contents

(36 pages in total)

List of symbols and abbreviation

a_{ff}	free-free flexibility matrix
$\boldsymbol{B}$	body force, e.g. due to gravity
$\boldsymbol{C}_A$	force coefficient
$\boldsymbol{C}_L$	lift coefficient
$\boldsymbol{C}_{MP}$	pitch moment coefficient
$\boldsymbol{F}$	net force applied to the structure
$\boldsymbol{F}_{\mathsf{A}}$	aerodynamic force on aerodynamic grids
$\boldsymbol{F}_{\mathsf{S}}$	structural force on structural nodes
$\mathcal{F}(Q, \boldsymbol{x})$	Euler/Navier-Stokes equations flux matrix
G	fluid/structure interpolation matrix
$\boldsymbol{h}$	surface deformation
$\boldsymbol{h}_{\mathsf{A}}$	surface deformation in aerodynamic model
$\boldsymbol{h}_{\mathsf{S}}$	surface deformation in structural model
K	stiffness matrix
L_{ref}	reference length
m_{ref}	reference mass
M_∞	freestream Mach number
$\boldsymbol{n}$	surface normal
Re_∞	freestream Reynolds number
$S(Q, \boldsymbol{x})$	source term of Euler/Navier-Stokes equations
Q	flow variables
$\boldsymbol{u}$	flow velocity
U_{R}	reduced velocity, see Eq. 6
v_{ref}	reference volume, defined here as L_{ref}^3
V^*	speed index, see Eq. 6
$\boldsymbol{x}$	vector representing the state of the structure
$\boldsymbol{x}_{\mathsf{J}}$	jig shape of the structure
α	angle-of-attack
δ_{H}	deflection of horizontal tail plane (HTP)
μ	mass ratio, see Eq. 6
ρ_∞	freestream density

This page is intentionally left blank.

1 Introduction

Historically, investigations into the field of aeroelasticity are often based on the application of linear, approximate aerodynamic methods. The advantages of these methods are easily understood, since it results into a linear set of equations. Solving the set of equations is straightforward and requires little computer turnaround time. Moreover, the linear set of equations also provides quick and easy calculation of derivatives of aerodynamic influence coefficients with respect to surface deformations. This allows for direct solution methods of static aeroelastic problems including trimming. The application of approximate aerodynamic methods also poses several disadvantages. Especially, the non-linear effects due to compressibility which increases the uncertainty of the method when applied in transonic speeds. Moreover, the representation of non-lifting surfaces of finite thickness is problematic.

In the development of aeroelastic approaches based on non-linear aerodynamic methods, NLR has worked on methods based on the full-potential equation 6, 8 and, more recently, on methods based on the Euler and Navier-Stokes equations 15, 16. These approaches are justified by the need to model non-linear compressibility effects for applications in transonic speed and by the need for high-fidelity aeroelastic analyses for modern, flexible aircraft and wind tunnel models, e.g. Refs. 1, 2, 5, 10, 12. In this respect, the influence of the structural deformation on aircraft performance, including the performance of high lift devices, is studied, see also the work of Chang et al. [2]. Also, many modern transport-aircraft designs incorporate wing tip devices. The investigation of the performance of such devices, in relation to aircraft flexibility, is currently a hot topic. Numerous recent studies incorporate the flexibility directly into the multidisciplinary design process, see e.g. Giunta and Sobieszczanski-Sobieski [3], Gumbert et al. [4], or even try to exploit the aeroelastic deformation to improve aircraft performance 9. Application to spacecraft 13 and to the problem of model deformations in wind tunnel are also reported, see e.g. Refs. 1, 5, 12. All these applications show that under certain conditions the accurate calculation of loads and deformations prevails over the quick but less accurate linear methods.

In the present work, the verification and validation of an enhanced aeroelastic approach, using aerodynamic methods based on the Euler and the Navier-Stokes equations, is presented. The test case for this work is found in the important effects of flight loads at manoeuvres on a high performance fighter aircraft 10, 16. A high load factor condition is typically associated with complex flow phenomena, such as vortices, strong shock waves, and possible shock-induced flow separation. Accurate and simultaneous predictions of loads and deformations at such conditions is used to support the complex investigations of several operational issues such as:

– fatigue life cycle assessment and maintenance scheduling;

– safety aspects;

– aircraft loads analysis;

– ageing aircraft monitoring;

– in flight deformation measurements analysis and verification;

– definition of desired support capabilities in the future.

In this paper, the focus is placed on description and application of the methodology as embedded in the NLR-developed ENFLOW computational aeroelastic system. Applications for an F-16 fighter aircraft are shown. A comparison is made with results of linear methods and preliminary results of flight test reported in Ref. 20.

2 Analysis method

In the present work, linear and nonlinear aerodynamic methods are employed in the aeroelastic simulations in conjunction with linear structural modelling. For the linear aerodynamic method the doublet lattice approach of MSC.NASTRAN is used while for the nonlinear aerodynamic method the NLR ENFLOW aeroelastic system is employed. The NLR ENFLOW system consists of components enabling common flow analyses about rigid configurations up to flow analyses with steady or time-accurate interaction with structural dynamics. The schematic diagram of the ENFLOW system is shown in 1. The components of ENFLOW system includes the domain modeller ENDOMO, the grid generator ENGRID, the flow solver ENSOLV and other supporting tools for geometry preprocessing and post processing of the results. The interaction with structural dynamics is handled by modules embedded within ENSOLV: a fluid-structure interaction module and a grid deformation module. The structural dynamic data can be derived from a model based on the finite element method (FEM), i.e. in the form of modal data (mode shapes, generalised masses, natural frequencies and modal damping coefficients) or data in the physical coordinates (mass matrix, stiffness matrix and damping matrix).

The flow solver of the ENFLOW system, i.e. ENSOLV, solves the Euler/Reynolds-Averaged Navier-Stokes (RANS) equations in multi-block structured grids. To model turbulent flows, several turbulence models are available including algebraic model and various variants of the $k - \omega$ two-equation model. An advanced option is also available consisting of hybrid large-eddy simulation (LES) and RANS called extra-large eddy simulation (XLES).

The ENFLOW system is currently the workhorse at NLR which is deployed for a wide range of investigations requiring high fidelity of CFD analyses: aerodynamic performance of aircraft configurations, aircraft-engine integrations, missile aerodynamics, unsteady flow about oscillating configurations, naturally unsteady flows, determination of wind tunnel support and wall interference, internal flow inside aircraft cabin, etc. Applications involving interactions with the flexibility of the aircraft structure are mostly for military purposes, e.g. flight load analyses of fighter aircraft, determination of flutter boundary, response analyses, etc.

2.1 Aerodynamic and structural modelling

The governing equations for a static aeroelastic system consist of the equations governing the flexibility of the structure and the equations governing the flow about the structure. Assuming that the deformation of the structure is relatively small, a linearised structural model may be employed.

The non-linear Euler/Navier-Stokes equations are used to model the flow around the structure. In the following, only the static aeroelastic equations will be considered In a non-dimensional form

the governing equations may be recast as:

$$Kh = 0.50\,V^{*\,2}C_A(Q, x) + B, \tag{1}$$

$$\frac{\partial Q}{\partial t} + \nabla \cdot \mathcal{F}(Q, x) = \mathcal{S}(Q, x), \tag{2}$$

These equations are coupled through the kinematic condition on the aero-structural interface. The inclusion of the time derivative in equation (2) is to facilitate the solution method exploiting the hyperbolic character of the unsteady form of Euler/Navier-Stokes equations. Let n be a vector normal to the aero-structural interface. The condition on the solid surface becomes:

$$u \cdot n(x) = 0, \quad \text{for inviscid flow}, \tag{3}$$

$$u = 0, \quad \text{for viscous flow}, \tag{4}$$

along with conditions for the other thermodynamic quantities, e.g. adiabatic wall. In equations (1) to (4) K is the stiffness matrix, B is the vector of body force and C_A is the vector of aerodynamic force coefficients which is a function of the vector of flow variable Q governed by the Euler/Navier-Stokes equations. $\mathcal{F}$ and $\mathcal{S}$ are the flux matrix and the source term of the Euler/Navier-Stokes equations. The position vector x and deformation h are defined as

$$x = x_{\mathsf{J}} + h, \tag{5}$$

where the subscript J refers to undeformed condition, i.e. the shape of the manufacturing jig. These variables may be defined in the aerodynamic or in the structural domain. Note that since linearity is assumed for the structural behaviour, the matrix K is constant.

In addition to the usual similarity parameters involved in aerodynamic analyses, e.g. Reynolds number Re_∞ and Mach number M_∞, aero-structural interaction parameters are also involved, i.e. the speed index V^* defined as:

$$V^* = U_{\mathsf{R}}/\sqrt{\mu}, \tag{6}$$

with reduced velocity $U_{\mathsf{R}} = u_\infty/(\omega_{\mathsf{ref}} L_{\mathsf{ref}})$ and mass ratio $\mu = m_{\mathsf{ref}}/(\rho_\infty v_{\mathsf{ref}})$. These similarity parameters are invariant across the aero-structural boundary and therefore are used as synchronisation parameters between the aerodynamic and structural solution procedure. Note that although a steady flow problem is involved, a time parameter (ω_{ref}) has been used. This is to maintain compatibility with the dynamic case.

2.2 Solution method

The set of aeroelastic equations (1) and (2) are solved in a loosely-coupled manner 14, 16, i.e. (1) using relatively distinct solution procedures for the aerodynamic and structural part and (2) applying space and time synchronisation between the parts. The first aspect would allow the approach to take full advantage of the available optimised solution methods, in practice the available codes, for each of the part. The second aspect is designed to model the interdependency between these parts.

The aerodynamic governing equations are solved using a finite-volume technique on structured multiblock grids. After space discretisation, using a second order central differencing, the following set of semi-discrete equations is obtained:

$$\frac{dQ_i}{dt} + R_i(Q, \boldsymbol{x}) = 0 \qquad i = 1..N_{\text{cell}}, \tag{7}$$

where Q_i is the approximation of Q at cell i and R_i is the residual of the discretised Euler/Navier-Stokes equations in cell i. As already mentioned previously, the unsteady form of equation (7) is to facilitate the solution of $R(Q, \boldsymbol{x}) = 0$ and not to capture the unsteady behaviour of the problems. A full approximation storage (FAS) multi-grid Runge-Kutta method is employed for the relaxation.

The structure of the aircraft is represented as a system with a finite number of degrees of freedom using a finite element method FEM. In the FEM approach elements are defined to represent the stiffness and inertia of the structure. These elements are then assembled to form the model of the whole aircraft. The commercial FEM package NASTRAN has been used throughout the investigation.

The interaction between the aerodynamic solution method ENSOLV and NASTRAN can be performed in two ways. First scheme is to tailor ENSOLV to produce input for NASTRAN in the form of concentrated forces at the nodes representing the aircraft surface in the FEM model. During one loop ENSOLV and NASTRAN are executed in sequence. The second scheme is to let NASTRAN compute the stiffness and inertia properties of the aircraft and feed the data into ENSOLV. The iteration loop can then be carried out within ENSOLV completely. The first scheme is only plausible when the structural model is nonlinear while the second scheme is more suitable for linear structural modelling. In the present work, is therefore, the second approach is used.

After the aerodynamic forces are determined through solution of the flow equations, the structural deformation can be calculated from:

$$\boldsymbol{h} = a\boldsymbol{F}, \qquad \text{where} \quad \boldsymbol{F} = 0.50\, V^{*2} \boldsymbol{C}_A(\boldsymbol{x}_{\text{J}} + \boldsymbol{h}) + \boldsymbol{B}, \tag{8}$$

and $a = K^{-1}$ is called the flexibility matrix or structural influence coefficient matrix. The body forces $\boldsymbol{B}$ are computed using the acceleration data at the structural node including the gravity.

When a linear lifting surface theory is used for the calculation of the aerodynamic forces the effect of wing camber, initial angle of attack and surface deformation are given as transpiration velocities on the lifting surface. In this case, the gradient of the aerodynamic force to the displacement, which is independent from the deformation, can be easily obtained. Equation (8) can then be solved in one step as:

$$\boldsymbol{h} = \tilde{a}\boldsymbol{F}_{\mathsf{J}}, \quad \text{where} \quad \boldsymbol{F}_{\mathsf{J}} = 0.50\,V^{*\,2}\boldsymbol{C}_A(\boldsymbol{x}_{\mathsf{J}}) + \boldsymbol{B}, \tag{9}$$

where $\tilde{a} = \tilde{K}^{-1}$ and $\tilde{K}$, also known as the aeroelastic deflection attenuation matrix, is:

$$\tilde{K} = K - 0.50\,V^{*\,2}\frac{\partial \boldsymbol{C}_A}{\partial \boldsymbol{x}}. \tag{10}$$

Note that the divergence speed index V_{d}^* is the speed index at which $\tilde{K}$ is singular, thereby the displacement is theoretically infinite. The divergence speed index can be computed by solving the eigenvalue problem $K - V_{\mathsf{d}}^{*\,2}[0.50\,\partial \boldsymbol{C}_A/\partial \boldsymbol{x}] = 0$. When the gradient of $\boldsymbol{C}_A$ to the change of surface geometry is difficult to obtain, as in the case of the Euler/Reynolds-Averaged Navier-Stokes equations, an approximation is sought. In the present study, a simple iterative scheme is used where:

$$\tilde{K} \approx K. \tag{11}$$

In other words, the second term of equation (10) is moved to the right-hand-side. The iteration scheme becomes:

$$\boldsymbol{h}^{p+1} = (1 - \omega)\boldsymbol{h}^p + \omega\,a\boldsymbol{F} \quad \text{where} \quad \boldsymbol{F} = 0.50\,V^{*\,2}\boldsymbol{C}_A(\boldsymbol{x}_{\mathsf{J}} + \boldsymbol{h}^p) + \boldsymbol{B}, \tag{12}$$

where p is the iteration counter, ω is an under-relaxation factor. The under-relaxation factor is added due to the approximation used for the gradient, i.e. equation (11). The solution of the aeroelastic system is obtained by an iteration of sequences of equation (7) and equation (12) until the changes of the deformation and aerodynamic forces fall below a certain tolerance.

During the iteration the aerodynamic state is updated as soon as the displacement of the solid boundary is obtained and the grid has been deformed using the method presented in section 2.4. Note that equation 12 is solved at the structural grid. Thus the aerodynamic force coefficient has to be transferred from to the aerodynamic grid to the structural grid to define the load on the structure. Subsequently the displacement obtained on the structural grid has to be transferred to the aerodynamic grid to determine the new position of the aerodynamic surface. The method used in the present study to transfer the data will be presented in the next section.

2.3 Aero-structural interpolation

One of the consequences in adopting a loosely-coupled approach is the difference in the aero-structural interface representation from the point of view of structural and aerodynamic solution method. Meanwhile, this interface is the contact surface between the aerodynamic and structural domain where deformations and forces are communicated. An interpolation method is therefore needed.

The displacement vector in the aerodynamic grid, h_A , can be expressed in terms of the displacement vector in the structural grid points, h_S, as

$$h_A = Gh_S \tag{13}$$

where G is the interpolation or spline matrix between the two surface grid systems. Requiring that the data exchange between the two domains conserves the virtual work, the point loads vector at structural grid, F_s, has to be computed from that at the aerodynamic grid as:

$$F_S = G^T F_A. \tag{14}$$

where F_A is the point loads vector at the aerodynamic grids. The spline matrix G is defined using global spline technique for which a function $f(x)$ is assumed to have the form of:

$$f(x) \approx \mathcal{P}(x) + \phi(r), \tag{15}$$

with $\mathcal{P}$ is a low order polynomial and ϕ is a radial function. Surface spline or volume spline methods are used in the present exercises. A detailed discussion on the numerical computation of G matrix can be found in Ref. 7.

Employment of a global interpolation methods ensure the continuity of the deformation on the aerodynamic grids. In some cases however, the structure consists of distinct components, e.g. main wing, flaps, elevator, etc. When these components are also represented as distinct components in the aerodynamic grid the interpolation process is then carried out component-wise. If necessary, the aerodynamic grid continuity between the components is maintained through enforcement of constraints.

2.4 Grid deformation technique

The present grid deformation method for structured multiblock grids is a combination of a volume spline technique and a transfinite interpolation (TFI) method. A multi-block grid consists of a set of three-dimensional blocks {B} bounded by six two-dimensional faces {F}. Each of the faces {F} are bounded by four one-dimensional edges {E}. At the ends of an edge two vertices {V} are defined.

The grid deformation method takes the deformations of the vertices which lie on the aero-structural interface as the input. During the first step, these deformations are interpolated into the edges in the field using the three-dimensional volume spline method 7. Subsequently, the deformations on the faces are computed using TFI based on the input of deformation of their bounding edges, which are either deformed by the volume spline during the first step or given as input in case they lie on the aero-structural interface. Finally, the face deformations, again which are either results from the second step or input from the aero-structural interface, are interpolated into the block interior using also a TFI technique, see Ref. 19 for a more detailed description.

2.5 Restrained simulation, free-free simulation and trimming procedure

Two types of static aeroelastic simulation can be carried out using the ENFLOW system, i.e. re-strained and free-flying. For the case of a wind tunnel model attached to the wind tunnel wall, the case is called a restrained case. The attachment provides the balancing forces and moments according to the aerodynamic and inertial loads working on the model. The modelling in static aeroelastic simulations is straight forward. Both inertial and aerodynamic forces are considered as external forces while appropriate boundary conditions are enforced at the attachment. The deformation of the structure due to external loads becomes:

$$h_{\mathsf{S}} = h_{\mathsf{F}} = a\boldsymbol{F}, \tag{16}$$

where a is the restrained flexibility matrix, h_{S} is the displacement of a structural node which consists of only the flexible deformation h_{F} and $\boldsymbol{F}$ is the total force acting on the structure which consists of aerodynamic force $\boldsymbol{F}_{\mathsf{A}}$ and inertial force $M\boldsymbol{g}$, g is gravitational acceleration.

For the case of a free-flying object like an aircraft, the inertial and the aerodynamic forces are in balance. This condition implies that when the aerodynamic force is given, e.g. by specifying a given angle of attack and Mach number, the acceleration of the aircraft may not be specified sep-arately. Instead, the acceleration should be calculated from the aerodynamic force and the inertia property of the aircraft. On the contrary, when the acceleration of the aircraft is specified, e.g. by specifying the load factor, the aerodynamic configuration should be sought at which the aerody-namic force will balance the inertial force resulting from the given acceleration. The method to satisfy the free-flying condition applied in the present work is the inertia-relief method, see e.g. Ref. 17, 18. In this method the inertial forces are directly related to the external forces, in this case the aerodynamic forces. With the help of the rigid body modes, the free-flying condition may be written as:

$$\phi_{\mathsf{R}}^{T}\left[\boldsymbol{F}_{\mathsf{A}} - M\,\phi_{\mathsf{R}}\,\ddot{\boldsymbol{q}}_{\mathsf{R}}\right] = 0, \tag{17}$$

where ϕ_R are the rigid body modes, M is the mass matrix and $\ddot{q}_\mathsf{R}$ is the generalised rigid body acceleration. Acceleration, expressed in the rigid body mode, is then sought which produces the required inertial forces to balance the external force.

$$\ddot{q}_\mathsf{R} = m_\mathsf{R}^{-1} \phi_\mathsf{R}^T \, \boldsymbol{F}_\mathsf{A}, \quad \text{where} \quad m_\mathsf{R} = \phi_\mathsf{R}^T \, M \, \phi_\mathsf{R}. \tag{18}$$

The total forces acting on the aircraft structure become:

$$\boldsymbol{F} = \mathcal{R}^T \, \boldsymbol{F}_\mathsf{A}, \quad \text{where} \quad \mathcal{R} = I - m_\mathsf{R}^{-1} \phi_\mathsf{R}^T \, M. \tag{19}$$

$\mathcal{R}$ is also known as the rigid body modifying matrix. The condition of statically balanced free-flight can be stated as a requirement for the mean axes such that the deformation occurring about them does not cause the centre of gravity to move and the axes to rotate, see Milne [11], Rodden and Love [18]. This requirement can be translated into the condition:

$$\phi_\mathsf{R}^T \, M \, \boldsymbol{h}_\mathsf{S} = 0, \quad \text{where} \quad \boldsymbol{h}_\mathsf{S} = \boldsymbol{h}_\mathsf{F} + \phi_\mathsf{R} \, q_\mathsf{R}, \tag{20}$$

M is the mass matrix and $\boldsymbol{h}_\mathsf{S}$ is the displacement of a structural point which consists of flexible component $\boldsymbol{h}_\mathsf{F}$ and rigid body component $\phi_\mathsf{R} \, q_\mathsf{R}$. One can work out equation (20) to obtain the relation between the generalised rigid body displacement q_R and the flexible deformation $\boldsymbol{h}_\mathsf{F}$ to obtain the displacement of a structural node

$$\boldsymbol{h}_\mathsf{S} = \mathcal{R} \, \boldsymbol{h}_\mathsf{F}. \tag{21}$$

Considering equation (16) the displacement of a structural point can be expressed as function of aerodynamic force only as:

$$\boldsymbol{h}_\mathsf{S} = a_\mathsf{FF} \boldsymbol{F}_\mathsf{A}, \quad \text{where} \quad a_\mathsf{FF} = \mathcal{R} \, a \, \mathcal{R}^T. \tag{22}$$

a_FF is called the free-free flexibility matrix.

The other aspect in a static aeroelastic simulation is the flow condition for the aerodynamic computation. Here, two possibilities are also available. First, when the flow condition is given, i.e. an angle-of-attack, a Mach number, etc., the acceleration acting on the aircraft is defined by equation (18). Second, when the acceleration of the aircraft is given, e.g. in terms of load factor, the aerodynamic force, or in practice the flow condition, corresponding to this acceleration has to be sought. For a static aeroelastic simulation using CFD, the first approach is straightforward while the second requires special treatment, i.e. trimming.

In a trimming process, the required forces and moments acting on the aircraft are first defined based on the inertia data, load factor, etc. Then a set of trim parameters are defined including their

limits, e.g. maximum flap deflection, minimum altitude, etc. An optimisation problem can then be defined with forces and moments as the objectives, trim parameters as the variables and the limits as the constraints. In the present work a simplified trimming process is employed where a target lift coefficient C_L^{T} and a pitching moment coefficient C_{MP}^{T} are defined along with two trim parameters, i.e. angle-of-attack α and the deflection of the horizontal stabiliser δ_{H}. Future work at NLR will employ a general trim analysis. The following trim equations can then be defined:

$$\left\{ \begin{array}{l} C_L(\alpha, \delta_{\mathsf{H}}) - C_L^{\mathsf{T}} \\ C_{MP}(\alpha, \delta_{\mathsf{H}}) - C_{MP}^{\mathsf{T}} \end{array} \right\} = 0, \tag{23}$$

to be solved for the trim variables $[\alpha, \delta_{\mathsf{H}}]^T$. Starting from a given initial state, the correction can be computed as

$$\left\{ \begin{array}{l} \Delta\alpha \\ \Delta\delta_{\mathsf{H}} \end{array} \right\} = \left[\begin{array}{cc} \partial C_L/\partial\alpha & \partial C_L/\partial\delta_{\mathsf{H}} \\ \partial C_M/\partial\alpha & \partial C_M/\partial\delta_{\mathsf{H}} \end{array} \right]^{-1} \left\{ \begin{array}{l} C_L - C_L^{\mathsf{T}} \\ C_M - C_M^{\mathsf{T}} \end{array} \right\}, \tag{24}$$

Similar to the case of static deformation (page 10), in case linear aerodynamic methods are used, the gradient matrix is constant and can be computed relatively easily. This gives the possibility to have a one step approach. In the present work the trim equations are solved in an iterative manner along with the flow equations and static deformation equations. These three sets of equations are solved in sequence which means that the coupling between these sets of equations are taken care of in a weak manner. As will be shown in the application section, this approach works fine for the present case.

3 Applications

Applications are presented for a free-flying F-16 aircraft in a simple air-to-air configuration. At the wing tip, i.e. stations 1 and 9, air-to-air missiles of type AIM-9J (SIDEWINDER) with the associated missile launchers (LAU-9) are attached. The other store attachment stations are empty. Figure 2 shows an overview of the geometry of the F-16 aircraft used in the present investigation. This configuration has been selected because it is one of the configurations tested by the Royal Netherlands Air Force (RNLAF) during a flight test campaign for maintenance investigation, see Ref. 20.

The required structural data, i.e. flexibility and mass matrices, are obtained with the help of NAS-TRAN finite element package. The desired data is acquired by executing NASTRAN for normal mode analysis where at certain stages of the computation the mass and stiffness matrices are written as extra outputs. The motivation of using the normal mode analysis of NASTRAN to extract the necessary data is the possibility to compare the natural frequencies and mode shapes computed by NASTRAN and those computed independently from the extracted data as a check. The commands to produce extra outputs are implemented using NASTRAN DMAP. The stiffness matrix is subsequently inverted and used as input for the ENFLOW system. When a restrained case is considered, a straight forward inversion can be carried out. Further processing can be performed to obtain a free-free flexibility matrix. For a free-free case, the degrees of freedom used to define the rigid body modes (the r-set in NASTRAN terms) are first separated from the other degrees of freedom (the l-set in NASTRAN terms). Further steps follow a similar way as the restrained case.

Structural properties of F-16 aircraft are represented by a combination of shell/plate elements (CQUAD4) with beam (CBEAM) and bar (CBAR) elements, see figure 3. This NASTRAN FEM model of the F-16 A/B aircraft was obtained from the manufacturer. The desired symmetrical free-flight configuration is modelled by putting constraints along the fuselage and defining the rigid body degrees of freedom (using SUPORT command) of normal translation and pitching rotation.

Static aeroelastic simulations have been carried out for a selected flight condition measured during the flight testing. The selected flight condition is a symmetrical pull-up manoeuvre at Mach 0.9 at altitude of 2,000 ft, called here flight level 20 (FL20). The fuel in the aircraft was 5,000 lbf. Continuous recording during the flight test was carried out from level flight up to a load factor of 8.

For the numerical simulation, conditions representing a load factor of 1, 2 and 4 have been computed. In these computations a free-flying condition is assumed. Two types of trim strategies have

been carried out: (i) trimming only on the lift force using the angle-of-attack as the variable and (ii) trimming on the lift force and pitching moment using the angle-of-attack and the deflection of horizontal stabiliser. Computations have been carried out using NASTRAN and ENFLOW system. For the computations using the NLR ENFLOW system the option of flow model based on the Euler equations is applied. The grid used for the computations is illustrated in Figure 5. The computational grid consists of about 2,5 million cells in 102 blocks. The NASTRAN results have been obtained using the static aeroelastic option (SOL 144). The aerodynamic panelling for the aerodynamic analysis using the doublet lattice method is shown in Figure 4. Angle of attack and horizontal stabiliser position have been used as the trim variables.

The deflection of the horizontal stabiliser is approximated using a continuous mode shape. This approach is applicable only for a relatively small deflection but found to be suitable for the present work. An example of a 10 degree nose-down deflection of the horizontal stabiliser is shown in Figure 6. The change in the angle of attack during simulations is effectuated by rotating the whole aircraft about its centre of gravity.

The static aeroelastic simulations have been executed on the NLR NEC SX5/8B computer. The flow equations, the structural equations and the trim equations are relaxed in a sequence, i.e. suspending the dependency between these sets of equations. The frequency of the structural and trim updates can be controlled freely. In the present work it is set to be once in every multi-grid cycle. The simulations are stopped after residual of the aerodynamic equations have been dropped at least 2 order of magnitude and convergence is obtained (usually up to 4 digits after decimal point) for the lift coefficient, the moment coefficients and the deflection. Each simulation usually takes about 20 minutes to converge on 4 processors of SX5/8B computer. Example of the history of the deflection extrema, trim variables, trim targets and the aerodynamic residual is presented in Figures 7, 8 and 9, respectively. As can be seen in these figures, the set of the aerodynamic equations, the structural equations and the trim equations converge almost simultaneously. This justifies the iteration method used in the present work.

The results of ENFLOW and NASTRAN in terms of the trim variables, i.e. the angle of attack α and the deflection of the horizontal stabiliser δ_H, are presented in Table 1 for the $[C_L] - [\alpha]$ trim strategy and Table 2 for the $[C_L, C_{MP}] - [\alpha, \delta_H]$ trim strategy. The values of the trim angle of attack and the deflection of the horizontal stabiliser computed using NASTRAN clearly show the linear behaviour of NASTRAN with respect to the load factor. It also shows that the NASTRAN aerodynamic panelling does not take into account the non-symmetry of the configuration, i.e. zero lift at zero angle of attack. Note that the NASTRAN model has been mostly employed for flutter analysis which justifies such aerodynamic panelling. The trim angle of attack computed using

ENFLOW depart slightly from linear behaviour with respect to the load factor. The deflection of the horizontal stabiliser computed using ENFLOW however, does not show linear behaviour with respect to the load factor. This may be explained that the deflection of the horizontal stabiliser is strongly associated with the pitching moment of the aircraft which is known to be non-linear in transonic flow, e.g. influenced by the shock position.

The pressure distribution on the upper surface of the aircraft is shown in Figures 10 to 12. Note that since symmetric cases are considered, the computations have been carried out for a half aircraft. Figures 10 to 12 show both results of simulation with $[C_L] - [\alpha]$ trim strategy, as the starboard half, and with $[C_L, C_{MP}] - [\alpha, \delta_H]$ trim strategy, as the portside half. The aircraft jig shape at zero angle of attack is also plotted for reference. As previously mentioned, the angle of attack is adjusted by rotating the whole aircraft about the centre of gravity. Due to the differences in the trim angle of attack between the results with $[C_L] - [\alpha]$ trim strategy and the results with $[C_L, C_{MP}] - [\alpha, \delta_H]$ trim strategy, discontinuity can be clearly seen at the centre of the aircraft. Inspecting the contours of the pressure, one can conclude that with the increase of the angle of attack, the shock position does not shift significantly. The region with negative pressure coefficient (suction) on the upper surface broadens and the level rises with the increase of the angle of attack.

The vertical deflection of the front spar and the rear spar computed using NASTRAN and ENFLOW is presented in Figure 13 for $n_z = 1$, Figure 14 for $n_z = 2$, and Figure 15 for $n_z = 4$. These deflections are the results of simulations incorporating $[C_L, C_{MP}] - [\alpha, \delta_H]$ trim strategy. The twist deformation with respect to the jig shape is presented in the next figures, i.e. Figure 16 for $n_z = 1$, Figure 17 for $n_z = 2$, and Figure 18 for $n_z = 4$. Differences between NASTRAN results and ENFLOW results are observed for both the vertical deflection and the twist deflection. Concerning the the twist deflection, the discrepancy may be attributed to the differences in the local aerodynamic loading between NASTRAN and ENFLOW. In case of ENFLOW the supersonic region and the strong shock waves generate relatively strong rear loading causing nose down twist deflection. The lifting surface of NASTRAN, on the other hand, will create strong suction close to the leading edge causing nose up twist deformation. This difference can be clearly seen from Figure 19 where comparison is made for the lifting pressure at 78% span between the results of NASTRAN and the results of ENFLOW. By increasing the load factor, the rear loading in the ENFLOW results and the front loading in the NASTRAN results increase accordingly. This leads to an opposite tendency for an increasing load factor, see Figures 16 to 18. Concerning the differences in the vertical deflection two possible explanations can be indicated. First, the differences in the pitching moment characteristic of the aircraft implies also different lift at the wing due to differences in the trimming force. As previously mentioned, ENFLOW results exhibit relatively strong rear loading at the wing

which requires relatively large down force at the horizontal stabiliser to balance it. This means that greater lift is generated at the wing for simulation using ENFLOW compared to the simulation using NASTRAN. Second, the differences of the lift at the wing may be caused by a different ratio of fuselage lift to wing lift. The aerodynamic panelling of the fuselage in the NASTRAN model, i.e. using lifting surface element, can lead to a too-high fuselage lift implying too-low wing lift. These aspects are being be studied further.

To get the idea of the additional forces to balance the aircraft, comparisons have been made between the results of $[C_L] - [\alpha]$ trim strategy and the results of $[C_L, C_{MP}] - [\alpha, \delta_H]$ trim strategy. For the sake of conciseness only the results for $n_z = 2$ are presented. Figure 20 and Figure 21 show comparison of ENFLOW results between the two trim strategies for the vertical deflection of the front spar and rear spar and for the twist deflection, respectively. Comparison of the NASTRAN results are presented in Figure 22 and Figure 23. The results of ENFLOW clearly indicate the significant increase of vertical deflection when pitching moment is also trimmed. The level of vertical deflection for only lift force trimming is in a much better agreement with the NASTRAN results which confirms the aspect discussed in the previous paragraph. The results of NASTRAN exhibit insignificant effect of balancing the pitching moment. The twist deformation in both NASTRAN and ENFLOW results appear to be less sensitive to the trim strategy.

Finally, a preliminary comparison is made with the results of the flight test. It should be noted that the flight test campaign that has been carried out by the Royal Netherlands Air Force RNLAF in co-operation with NLR in measuring the wing deformation was directed towards feasibility study for the proposed measurement methods, see Ref. 20. Thus only a limited data is available. A series of measurement campaign is planned in the near future. Figure 24 shows the comparison of the ENFLOW results, the NASTRAN results, and the measured data for the vertical deflection at the front spar and the rear spar relative to the deformation at level flight ($n_z = 1$). Keeping in mind of various aspects are not taken into account in the simulations, the results show good agreement.

4   Concluding remarks

In this paper static aeroelastic analysis of fighter aircraft in transonic flow has been presented. Two methods are involved, ENFLOW computational aeroelastic simulation system and NASTRAN. Simulation using ENFLOW system has been carried out using flow modelling based on the Euler equations while NASTRAN applies linear lifting surface theory. Preliminary comparison has also been made with the flight test data. Based on the results presented in this paper the following conclusions may be drawn:

– The iteration procedure of the ENFLOW system for three sets of equations, i.e. the aerodynamic equations, the structural equations and the trim equations, works efficiently and robustly for the cases considered in this work. The present weak coupling treatment between these sets of equations seems to perform quite effectively provided enough under-relaxation factor is applied.

– As expected differences are observed between the results of NASTRAN and the results of EN-FLOW. The following sources of differences have been discussed:

· Differences the type of wing loading, i.e. rear loading for ENFLOW and front loading for NASTRAN. In transonic flows where strong shock wave exists at the wing, the aerodynamic modelling based on the Euler equations should give more realistic load distribution.
· Differences in the required force to trim the aircraft.
· Differences in the ratio between fuselage lift and the wing lift.

– Preliminary comparison of the computed results using NASTRAN and ENFLOW with flight test data show good agreement for vertical deformation relative to the deformation at level flight.

During the coarse of the study the following aspects have been indicated to deserve further scrutiny:

– Inclusion of a more realistic motion model in the simulations, e.g. the pitch rate, and/or time-accurate simulation.
– Improvement of the aerodynamic panelling in the NASTRAN model to include steady effects such as initial twist distribution along the span, camber, etc., so that better comparison can be carried out.

5 References

1. A.W. Burner, T. Liu, S. Garg, T.A. Ghee, and N.J. Taylor. Aeroelastic deformation measurements of flap, gap, and overhang on a semispan model. *Journal of Aircraft*, 38(6):1147–1154, 2001.

2. K.C. Chang, H.H. Chen, T. Tzong, and T. Cebeci. Prediction of aeroelastic effects of aircraft configurations including high lift systems. ICAS Paper 2000.275.1, ICAS, 2000.

3. A.A. Giunta and J. Sobieszczanski-Sobieski. Progress toward using sensitivity derivatives in a high-fidelity aeroelastic analysis of a supersonic transport. AIAA Paper 98-4763, AIAA, 1998.

4. C.R. Gumbert, G.J.-W. Hou, and P.A. Newman. Simultaneous Aerodynamic and Structural Analysis and Design Optimization (SASDO) for a 3-D Wing. AIAA Paper 2001-2527, AIAA, 2001.

5. J.R. Hooker, A.W. Burner, and R. Valla. Static aeroelastic analysis of transonic wind tunnel models using finite element methods. AIAA Paper 97-2243, AIAA, 1997.

6. M.H.L. Hounjet and B.J.G. Eussen. Outline and application of the NLR aeroelastic simulation method. In *Proceedings of 19th Congress of ICAS*, pages 1418–1441, Anaheim, 1994. ICAS, also NLR-TP-94422, NLR, 1994.

7. M.H.L. Hounjet and J.J. Meijer. Evaluation of Elastomechanical and Aerodynamic Data Transfer Methods for Non-planar Configurations in Computational Aeroelastic Analysis. In *Proceedings of 1995 CEAS International Forum on Aeroelasticity and Structural Dynamics*, pages 11.1–11.24, Manchester, 1995. Royal Aeronautical Society, also NLR-TP-95690, NLR, 1995.

8. M.H.L. Hounjet, B.B. Prananta, and B.J.G. Eussen. Frequency domain unsteady aerodynamics in/from aeroelastic simulation. In *Proceedings of 1999 International Forum on Aeroelasticity and Structural Dynamics*, Williamsburg, 1999. CEAS/AIAA/ICASE/NASA Langley, also NLR-TP-99256, NLR, 1999.

9. S.I. Kuzmina, G. Amiryants, J. Schweiger, J. Cooper M. Amprokidis, and O. Sensburg. Review and outlook on active and passive aeroelastic design concepts for future aircraft. ICAS Paper 2002.432.1, ICAS, 2002.

10. M. Love, T. De La Garza, E. Charlton, and D. Eagle. Computational aeroelasticity in high performance aircraft flight loads. ICAS Paper 2000.481.1, ICAS, 2000.

11. R.D. Milne. Some remarks on the dynamics of the deformable bodies. *AIAA Journal*, 6(3): 556–558, 1968.

12. L. R. Owens, Jr. and R. A. Wahls. Reynolds Number Effects on a Supersonic Transport at Subsonic High-Lift Conditions. AIAA Paper 2001-0911, AIAA, 2001.

13. R.K. Prabhu. Summary Report of the Orbital X-34 Wing Static Aeroelastic models using finite element methods. NASA CR 2001-210850, NASA, 2001.

14. B.B. Prananta and M.H.L. Hounjet. Large time step aero-structural coupling procedures for aeroelastic simulation. In *Proceedings of 1997 CEAS International Forum on Aeroelasticity and Structural Dynamics*, volume 2, pages 63–71, Rome, 1997. Associazione Italiana di Aeronautica ed Astronautica, also NLR-TP-97619, NLR, 1997.

15. B.B. Prananta, J.C. Kok, S.P. Spekreijse, M.H.L. Hounjet, and J.J. Meijer. Simulation of limit cycle oscillation of fighter aircraft at moderate angle of attack. In *Proceedings of 2003 CEAS International Forum on Aeroelasticity and Structural Dynamics*, Amsterdam, 2003. National Aerospace Laboratory NLR.

16. B.B. Prananta, I W. Tjatra, S.P. Spekreijse, J.C. Kok, and J.J. Meijer. Static aeroelastic simulation of military aircraft configuration in transonic flow. In *Proceedings of International Forum on Aeroelasticity and Structural Dynamics, June 4-6 2001*. AIAE, also NLR-TP-2001-346, NLR, 2001.

17. W.P. Rodden and E.H. Johnson. *MSC/NASTRAN Aeroelastic Analysis User's Guide*. MacNeal-Schwendler Corporation, USA, 1994.

18. W.P. Rodden and J.R. Love. Equations of motion of a quasisteady flight vehicle utilizing restrained static aeroelastic characteristics. *AIAA Journal*, 22(9):802–809, 1979.

19. S.P. Spekreijse, B.B. Prananta, and J.C. Kok. A simple, robust and fast algorithm to compute deformations of multi-block structured grids. NLR Report TP-2002-105, NLR, 2002.

20. S Storm van Leeuwen. Military aircraft add-on certification in the Netherlands. In *Proceedings of 2003 CEAS International Forum on Aeroelasticity and Structural Dynamics*, Amsterdam, 2003. National Aerospace Laboratory NLR.

6   Figures and tables

load factor	α_{T}	
	ENFLOW	NASTRAN
$n_{\mathsf{z}} = 1$	0.5075	0.7264
$n_{\mathsf{z}} = 2$	1.1364	1.4527
$n_{\mathsf{z}} = 4$	2.3766	2.9055

Table 1   Comparison of trim variables between ENFLOW and NASTRAN for cases incorporating $[C_L] - [\alpha]$ trim strategy

load factor	α_{T}		$\delta_{\mathsf{H}\,\mathsf{T}}$	
	ENFLOW	NASTRAN	ENFLOW	NASTRAN
$n_{\mathsf{z}} = 1$	1.0349	0.7265	-3.4962	-0.0013
$n_{\mathsf{z}} = 2$	1.6933	1.4531	-4.2322	-0.0026
$n_{\mathsf{z}} = 4$	3.0155	2.9062	-5.1428	-0.0051

Table 2   Comparison of trim variables between ENFLOW and NASTRAN for cases incorporating $[C_L, C_{MP}] - [\alpha, \delta_{\mathsf{H}}]$ trim strategy
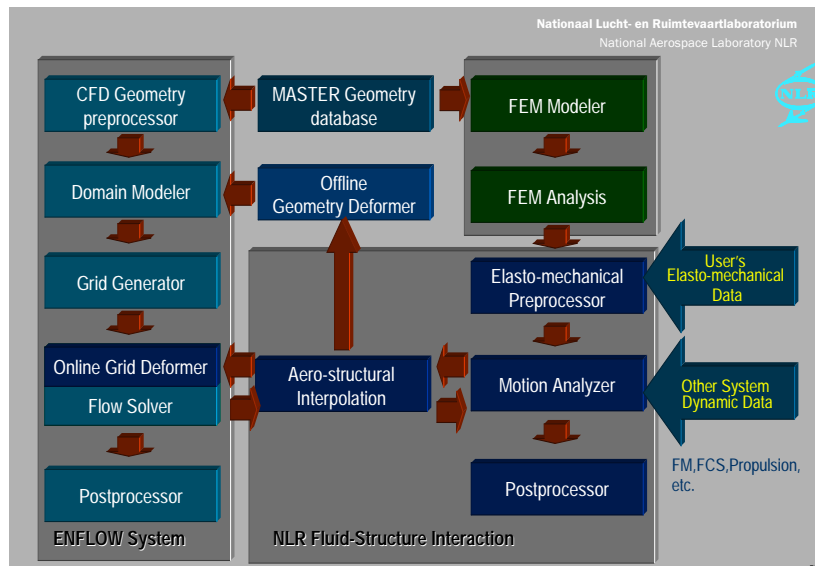
Fig. 1   *A schematic diagram of the* NLR *computational aeroelastic simulation (*CAS*) system employing the Euler/Navier-Stokes equations*
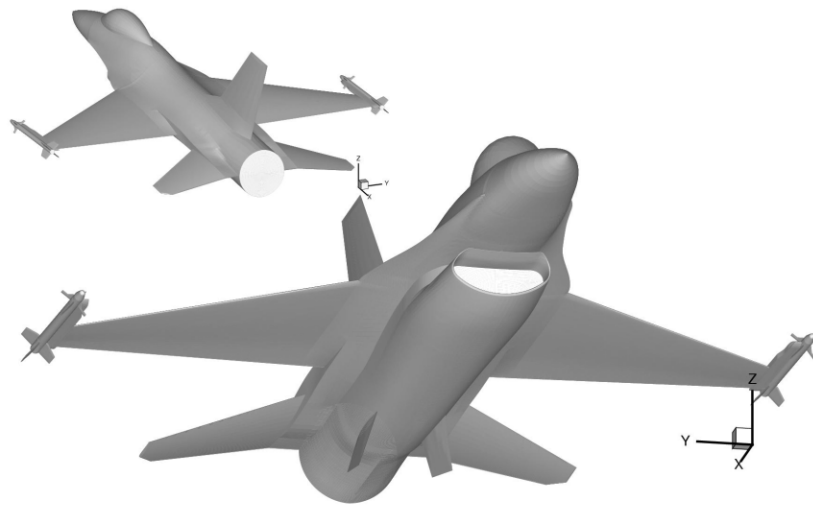
Fig. 2   Overview of the surface modelling of F-16 *aircraft with* SIDEWINDER *missiles on the wing
tip used in the present work*
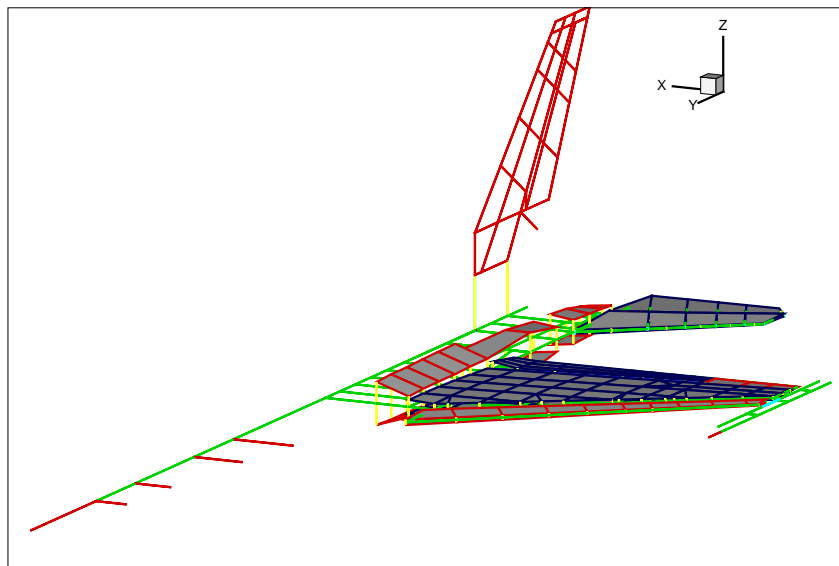
Fig. 3   Overview of the dynamic FEM *model of* F-16 *aircraft with* SIDEWINDER *missiles on the
wing tip used in the present work*
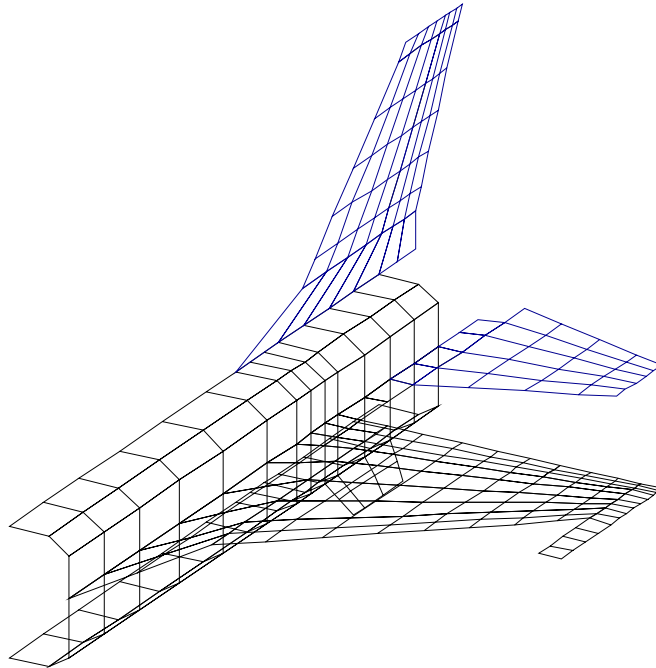
Fig. 4   Aerodynamic panelling for NASTRAN *static aeroelastic analysis, note the body is also represented as a lifting surface*
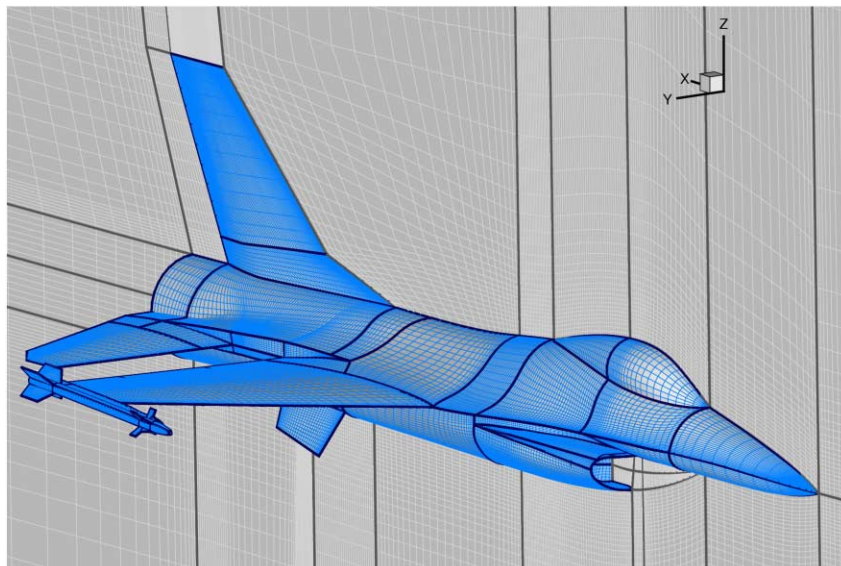
Fig. 5   Overview of the grid about F-16 *aircraft with* SIDEWINDER *missiles on the wing tip used in the present work*
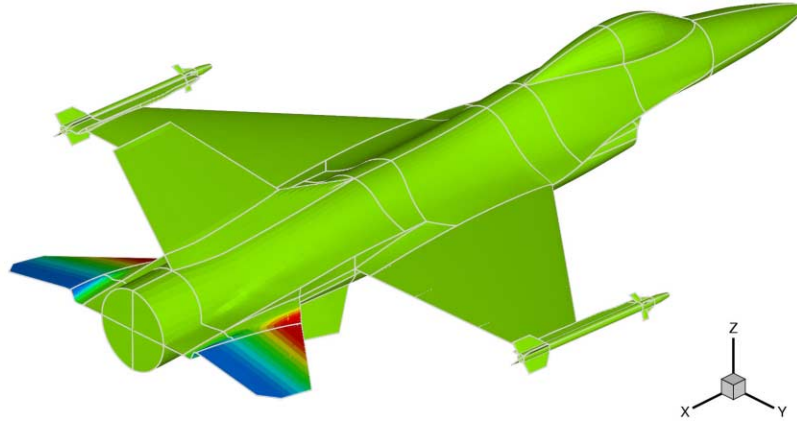
Fig. 6   Example of the deflection of horizontal stabiliser using a continuous mode shape, the depicted deflection is 10 degree nose-down
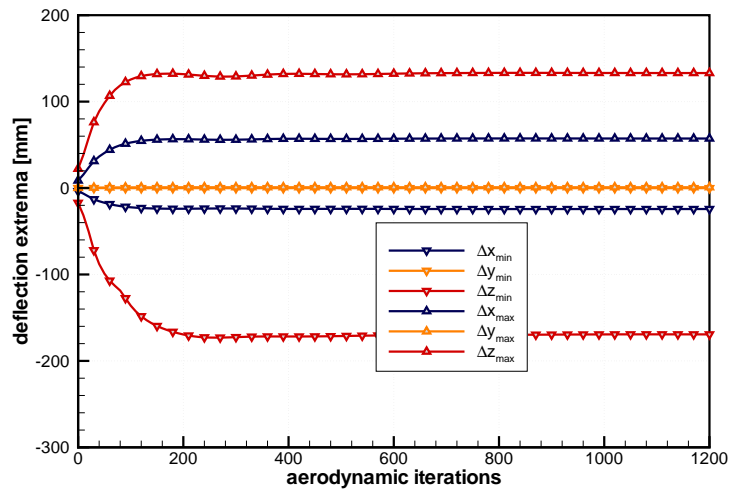
Fig. 7   History of deflection extrema during the iteration process, F-16 *with* SIDEWINDER *missile at the tip,* $n_z = 1$, $M_\infty = 0.9$, FL20 *altitude,* $[C_L, C_{MP}] - [\alpha, \delta_H]$ *trim strategy, flow model based on the Euler equations*
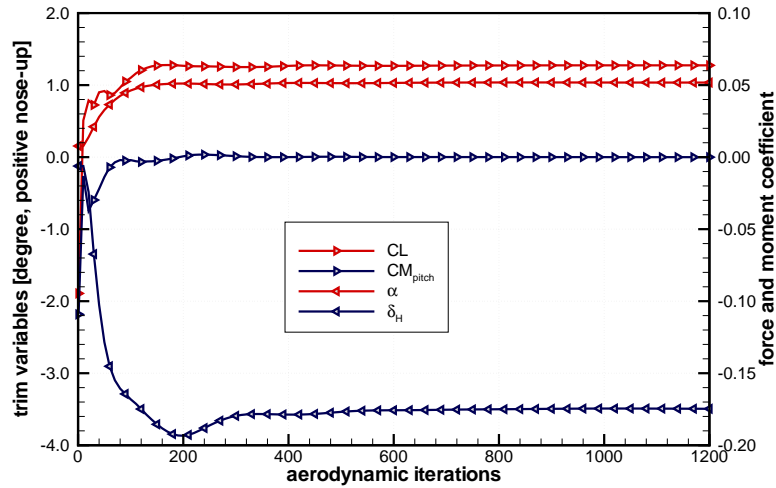
Fig. 8   History of trim variables and trim targets during the iteration process, F-16 *with* SIDEWINDER *missile at the tip,* $n_z = 1$, $M_\infty = 0.9$, FL20 *altitude,* $[C_L, C_{MP}] - [\alpha, \delta_H]$ *trim strategy, flow model based on the Euler equations*
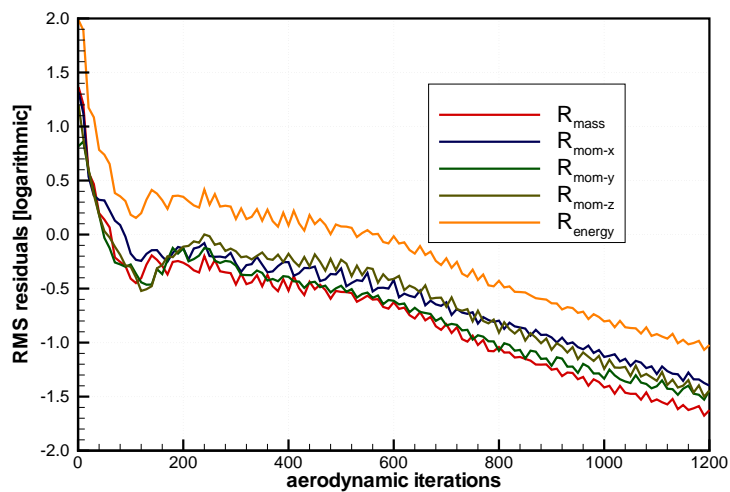
Fig. 9   History of the residual of the Euler equations during the iteration process, F-16 *with* SIDEWINDER *missile at the tip,* $n_z = 1$, $M_\infty = 0.9$, FL20 *altitude,* $[C_L, C_{MP}] - [\alpha, \delta_H]$ *trim strategy*
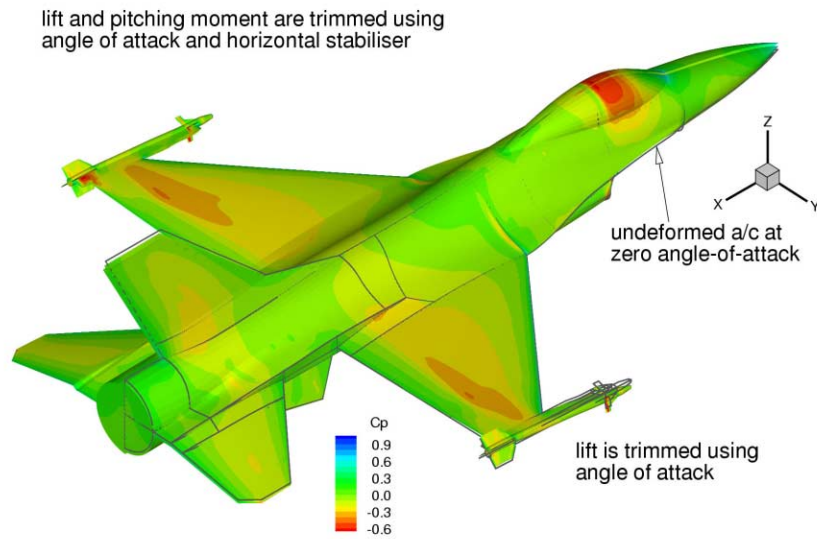
Fig. 10   Surface pressure distribution on deformed F-16 *aircraft with* SIDEWINDER *missile at the tip,* $n_z = 1$, $M_\infty = 0.9$, FL20 *altitude, the starboard shows the result of* $[C_L] - [\alpha]$ *trim strategy and the portside shows the result of* $[C_L, C_{MP}] - [\alpha, \delta_H]$ *trim strategy, flow model based on the Euler equations*
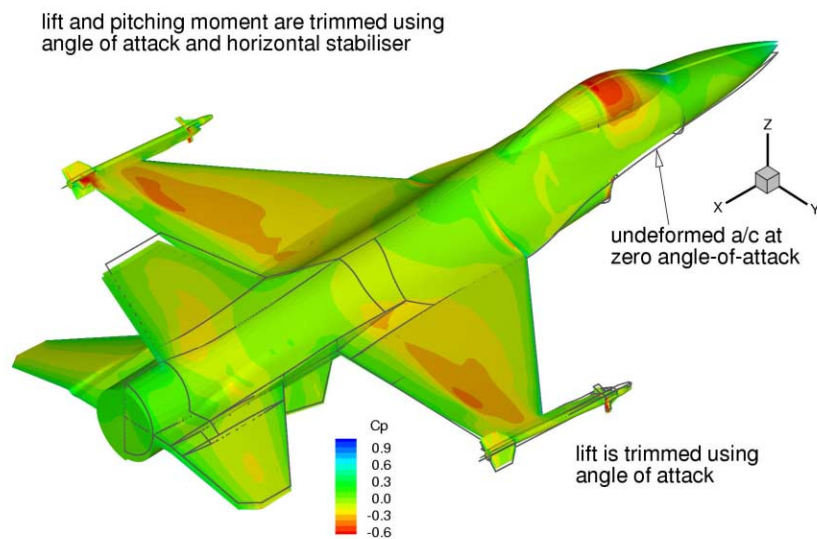
Fig. 11   Surface pressure distribution on deformed F-16 *aircraft with* SIDEWINDER *missile at the tip,* $n_z = 2$, $M_\infty = 0.9$, FL20 *altitude, the starboard shows the result of* $[C_L] - [\alpha]$ *trim strategy and the portside shows the result of* $[C_L, C_{MP}] - [\alpha, \delta_H]$ *trim strategy, flow model based on the Euler equations*
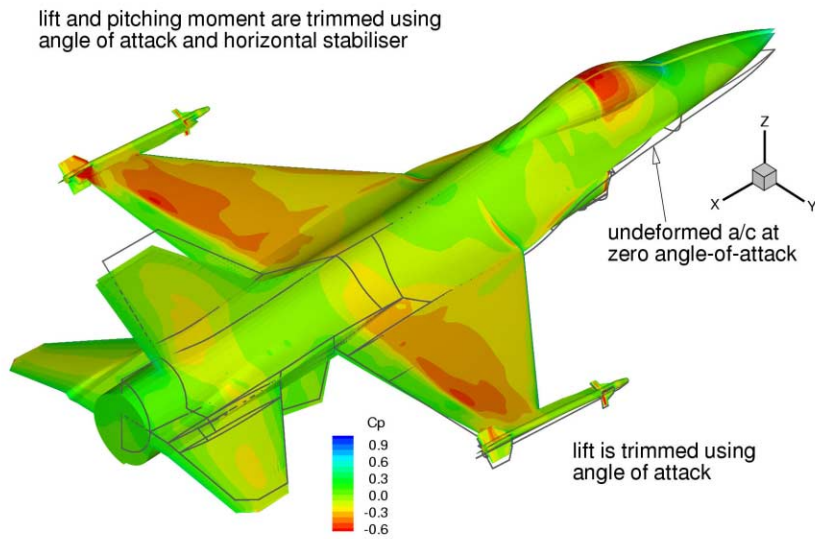
Fig. 12   Surface pressure distribution on deformed F-16 *aircraft with* SIDEWINDER *missile at the tip,* $n_z = 4$, $M_\infty = 0.9$, FL20 *altitude, the starboard is the result of* $[C_L] - [\alpha]$ *trim strategy and the portside is the result of* $[C_L, C_{MP}] - [\alpha, \delta_H]$ *trim strategy, flow model based on the Euler equations*
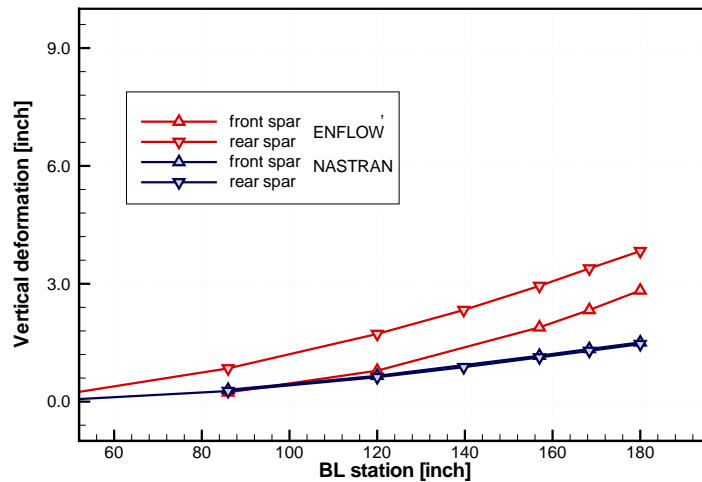
Fig. 13   Comparison of the results between NASTRAN *(doublet lattice) and* ENFLOW *(Euler equations) for the vertical deflection along the span,* F-16 *with* SIDEWINDER *missile at the tip,* $n_z = 1$, $M_\infty = 0.9$, FL20 *altitude*
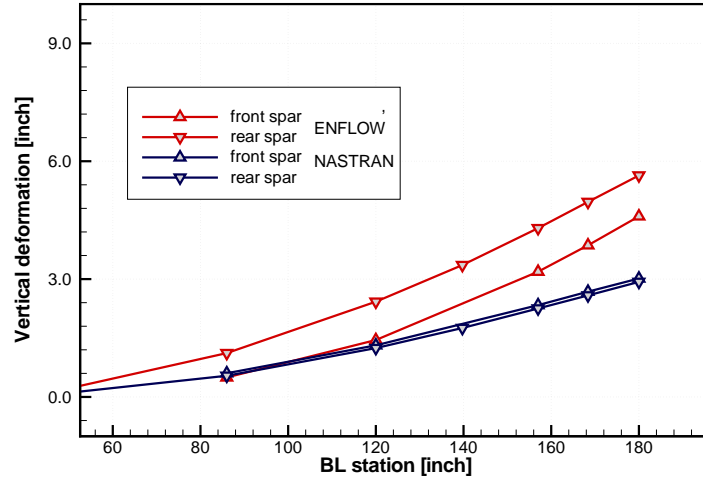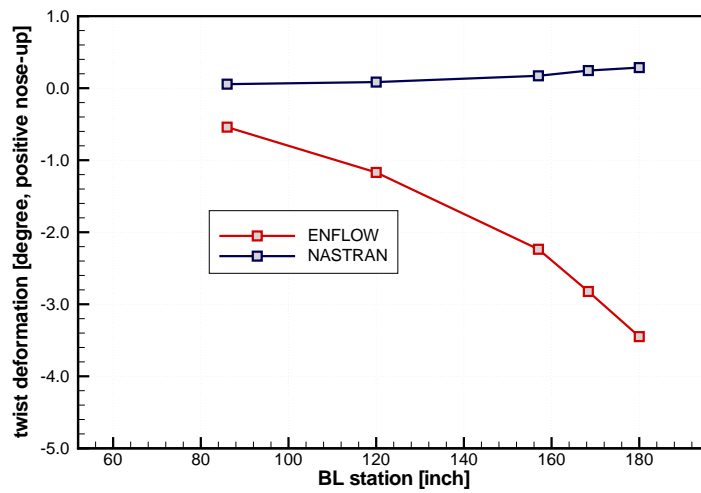
Fig. 14 Comparison of the results between NASTRAN *(doublet lattice) and* ENFLOW *(Euler equations) for the vertical deflection along the span,* F-16 *with* SIDEWINDER *missile at the tip,* $n_z = 2$, $M_\infty = 0.9$, FL20 *altitude*
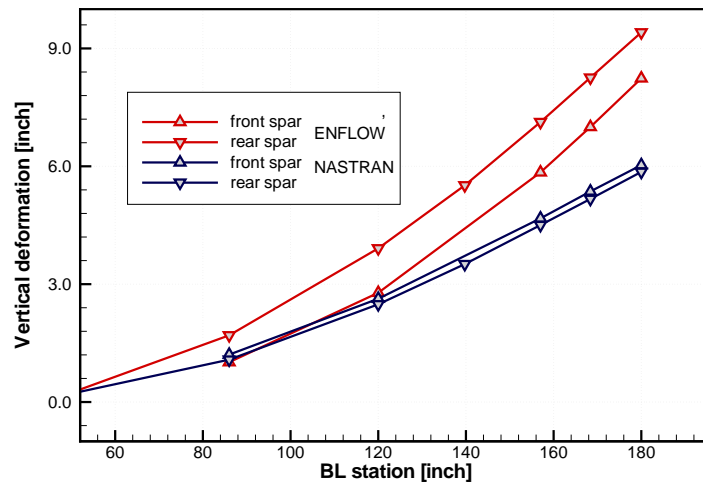
Fig. 15 Comparison of the results between NASTRAN *(doublet lattice) and* ENFLOW *(Euler equations) for the vertical deflection along the span,* F-16 *with* SIDEWINDER *missile at the tip,* $n_z = 4$, $M_\infty = 0.9$, FL20 *altitude*
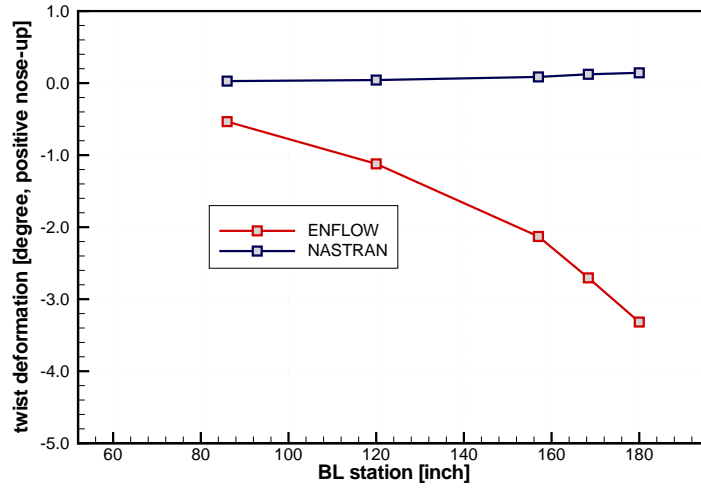
Fig. 16   Comparison of the results between NASTRAN (based on doublet lattice method) and
ENFLOW (solving the Euler equations) for the twist deflection along the span, F-16 with
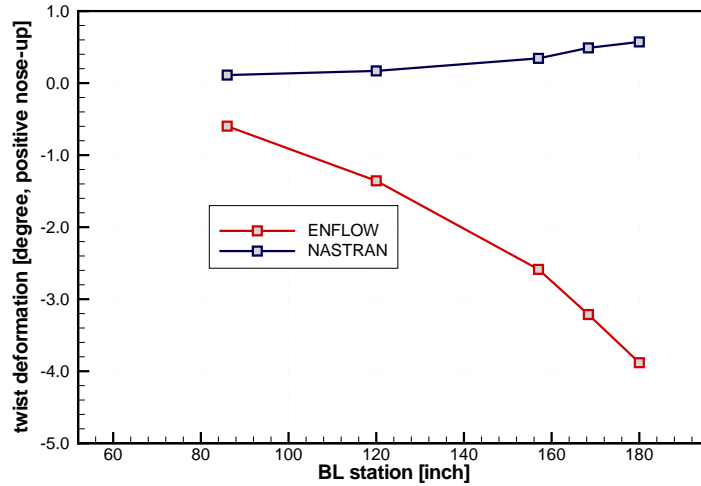SIDEWINDER missile at the tip, $n_z = 1$, $M_\infty = 0.9$, FL20 altitude

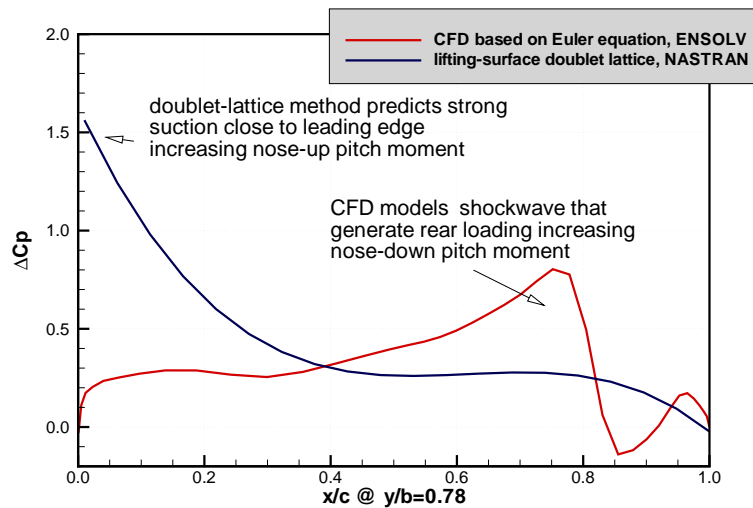Fig. 17   Comparison of the results between NASTRAN (doublet lattice) and scenflow (Euler
equations) for the twist deflection along the span, F-16 with SIDEWINDER missile at
the tip, $n_z = 2$, $M_\infty = 0.9$, FL20 altitude

Fig. 18   Comparison of the results between NASTRAN *(doublet lattice) and scenflow (Euler equations) for the twist deflection along the span,* F-16 *with* SIDEWINDER *missile at the tip,* $n_z = 4$, $M_\infty = 0.9$, FL20 *altitude*

Fig. 19   Comparison of the lifting pressure (ΔCp) at y/b=0.78 between NASTRAN *(doublet lattice) and* ENFLOW *(Euler equations),* F-16 *with* SIDEWINDER *missile at the tip,* $n_z = 4$, $M_\infty = 0.9$, FL20 *altitude*
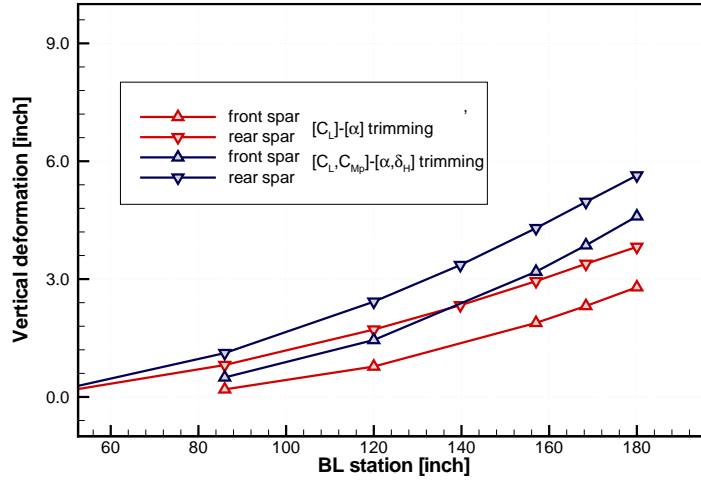
Fig. 20   Comparison of the ENFLOW results between $[C_L] - [\alpha]$ trim strategy and $[C_L, C_{MP}] - [\alpha, \delta_\mathsf{H}]$ trim strategy for the vertical deflection along the span, F-16 with SIDEWINDER missile at the tip, $n_\mathsf{z} = 2$, $M_\infty = 0.9$, FL20 altitude, flow model based on the Euler equations
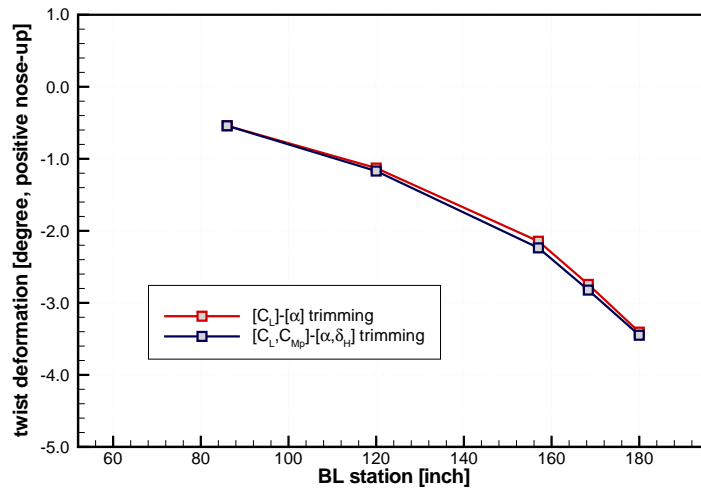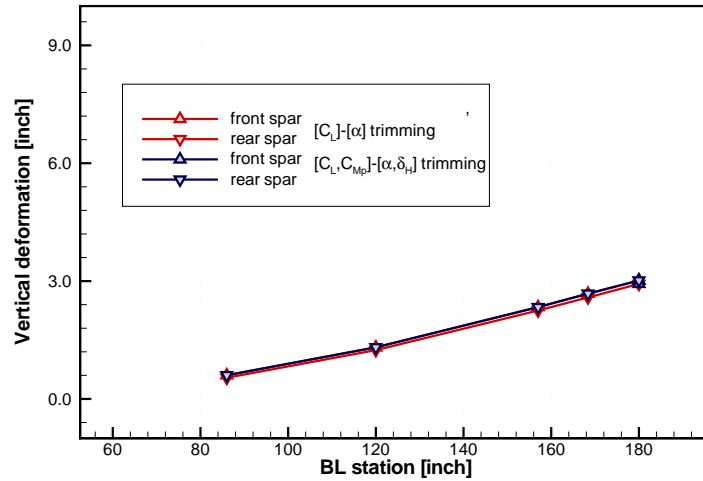

Fig. 21   Comparison of the ENFLOW results between $[C_L] - [\alpha]$ trim strategy and $[C_L, C_{MP}] - [\alpha, \delta_\mathsf{H}]$ trim strategy for the twist deflection along the span, F-16 with SIDEWINDER missile at the tip, $n_\mathsf{z} = 2$, $M_\infty = 0.9$, FL20 altitude, flow model based on the Euler equations

Fig. 22 Comparison of the NASTRAN *results between* $[C_L] - [\alpha]$ *trim strategy and* $[C_L, C_{MP}] - [\alpha, \delta_H]$ *trim strategy for the vertical deflection along the span,* F-16 *with* SIDEWINDER *missile at the tip,* $n_z = 2$, $M_\infty = 0.9$, FL20 *altitude, doublet lattice flow model*
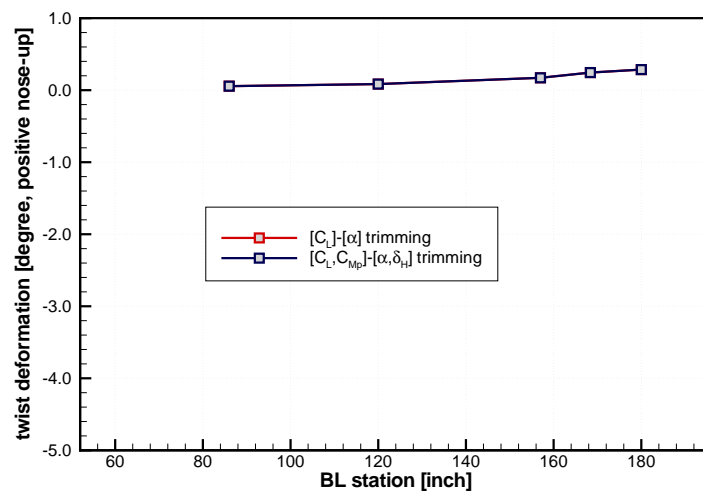

Fig. 23 Comparison of the NASTRAN *results between* $[C_L] - [\alpha]$ *trim strategy and* $[C_L, C_{MP}] - [\alpha, \delta_H]$ *trim strategy for the twist deflection along the span,* F-16 *with* SIDEWINDER *missile at the tip,* $n_z = 2$, $M_\infty = 0.9$, FL20 *altitude, doublet lattice flow model*
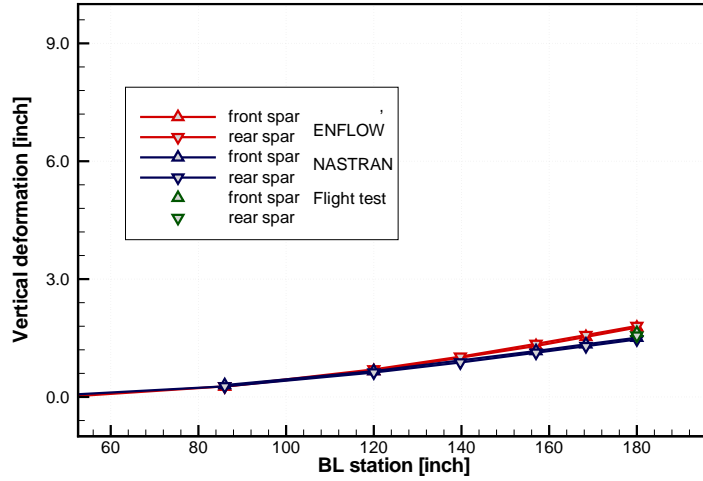
Fig. 24 *Comparison of the results between* NASTRAN *(doublet lattice),* ENFLOW *(Euler equations) and flight test for the vertical deflection along the span relative to the deflection at level flight,* F-16 *with* SIDEWINDER *missile at the tip,* $n_z = 2$, $M_\infty = 0.9$, FL20 *altitude*